ELSEVIER

Journal of Molecular Structure: THEOCHEM 806 (2007) 121–129

THEO CHEM

www.elsevier.com/locate/theochem

An ab initio dynamics study on the reaction of O(^{3}P) with $CH_3CH{=}CH_2$ (^{1}A′)

Weichao Zhang *, Benni Du, Changjun Feng

Department of chemistry, Xuzhou Normal University, Xuzhou, Jiangsu 221116, People's Republic of China

Received 28 September 2006; received in revised form 14 November 2006; accepted 14 November 2006
Available online 19 November 2006

Abstract

The reaction of O(^{3}P) with propene on the triplet potential energy surface is investigated using the unrestricted second-order Møller–Plesset perturbation (UMP2) and QCISD(T)/6-311++G(3df,2p) level methods. The calculational results indicate that the initial step of the reaction consists of an attachment of the electrophilic O(^{3}P) atom to both the carbon atoms of the double bond to form lower-energy intermediates IM1 and IM2. Among all these reaction channels the formation of $CH_2C(O)H+CH_3$ from IM2 is the dominant one and the products of CH_3COCH_2+H from IM2 and $CH_3CHC(O)H+H$ from IM1 are the secondary ones. The conventional transition state calculations are carried out with Wigner's tunneling correction at 298–500 K. The rate constants and activation energy calculated at the QCISD(T)/6-311++G(3df,2p) level within the range of temperature 298–500 K are in good agreement with the experimental values.

Keywords: Propene; QCISD(T); Reaction mechanism; Rate constants

1. Introduction

More attention has been paid to the reactions of O(^{3}P) with olefins for their importance in our understanding the combustion processes and oxidation mechanisms of hydrocarbon [1–11], among which the reaction of O(^{3}P) with propene has recently attracted much experimental attention [7–9]. Luntz's group [7] detected the product $CH_2C(O)H$ in the crossed molecular beam reaction of O(^{3}P) with propene using Laser-induced fluorescence (LIF) technique. Bersohn's group [8] investigated the H and $CH_2C(O)H$ products of the O(^{3}P) atom with propene by LIF method under single-collision conditions and the relative yield of $CH_2C(O)H$ radical in contrast to H atom is about 3. Su and Bersohn [9] studied the formation of vinoxy radicals $CH_2C(O)H$ in the reactions of O(^{3}P) with propene isotopomers. Besides these reaction mechanism investigations, the rate constants for the title reaction were also studied [12–14]. Knyazev's group [12] detected the rate for this reaction at room temperature under discharge flow conditions by resonance fluorescence spectroscopy of O and H atoms. The total rate constant of the reaction was detected as $(4.35 \pm 0.35) \times 10^{-12}$ cm^3 molecule^{-1} s^{-1}. Klemm et al. [13] studied the primary product of CH_3 in the $O+C_3H_6$ reaction using mass spectrometric detection via direct photoionization and the branching fraction for the formation of CH_3(d[CH_3]/d[O]) was detected. Arutyunov et al. [14] reported the contribution of H-producing channels to the reaction of O(^{3}P) with propylene was 46% at low pressure, and this figure decreased at higher pressures. This result showed that the H-producing channels can not be neglected.

The reactions of O(^{3}P) with ethylene and butene (or isobutene) have been studied theoretically [10,11], however, the reaction of O(^{3}P) with propene, as far as I know, has not yet been investigated theoretically. In this paper, we present an extensive theoretical study of the title reaction. The detailed reaction mechanism is revealed for the first time.

* Corresponding author. Tel.: +86 516 3403165; fax: +86 516 83403164.
E-mail address: zwc@xznu.edu.cn (W. Zhang).

0166-1280/$ - see front matter © 2007 Published by Elsevier B.V.
doi:10.1016/j.theochem.2006.11.014

2. Computational methods

Local minima and transition structures (TS) on the potential energy surface (PES) are initially optimized at the level of UMP2(full)/6-311G(d,p) [15]. Analytical harmonic vibration frequencies are computed at this level in order to verify the character of the stationary points located (one imaginary frequency for a TS and all real frequencies for a minimum) and to obtain the zero-point energies. An IRC calculation [16] is carried out for each transition state to confirm that it connects the desired reactant and product. To obtain high-quality energetic data, the following scheme is used to estimate the total energy at the QCISD(T)/6-311++G(3df,2p) level: E[QCISD(T)/6-311++G(3df,2p)] ≈ E[QCISD(T)/6-311G(d,p)] + E[UMP2/6-311++G(3df,2p)] − E[UMP2/6-311G(d,p)]

All ab initio calculations are carried out using the Gaussian98 program [17].

3. Results and discussion

The geometries of the reactants, intermediates and transition states involved in the $O(^3P)+CH_3CH{=}CH_2$ reaction are shown in Fig. 1. The relative energies (relative to reactants of $O(^3P)+CH_3CH{=}CH_2$) of all species calculated at different levels are summarized in Table 1. All of the imaginary frequencies of the transition states are listed in Table 2. Finally, schematic energetic profile of the triplet PES on the QCISD (T)/6-311++G(3df,2p) level for $O(^3P)+CH_3CH{=}CH_2$ reaction pathways is plotted in Fig. 2.

3.1. potential energy surface

For one of the reactants of $O(^3P)$ atom, different ways of its attacking at $CH_3CH{=}CH_2$ molecule will result in different products. The $O(^3P)$ atom may either abstract a H atom or make electrophilic addition to the double bond of the $CH_3CH{=}CH_2$ molecule. These processes take place on the triplet potential energy surface corresponding to the spin-conservation rule.

The $O(^3P)$ atom is an electrophilic atom. According to the Mulliken's atomic charges analysis of $CH_3CH{=}CH_2$ at the UMP2(full)/6-311G(d,p) level, the charges on the unsaturated C atoms in CH and CH_2 groups are −0.182 and −0.205, respectively. So the addition of $O(^3P)$ can occur at either carbon atom of the double bond of the propene, and the two possible addition pathways are considered first.

When $O(^3P)$ atom attacks the methylene carbon atom of the propene molecular, the intermediate IM1 is formed via the transition state TS1. On the other hand, if $O(^3P)$ atom is added to the methyne carbon atom of the propene molecular, the intermediate IM2 will be formed via TS2. The relative energies of TS1 and TS2 are only 0.51 and 0.57 kcal/mol, respectively, above the initial reactants calculated at the QCISD(T)/6-311++G(3df,2p) level of theory. This result is consistent with the experimental results of Su and Bersohn. [9] who investigated the mechanisms of formation of vinoxy radicals in the reaction of $O(^3P)$ with terminal alkenes and found that the vinoxys originated with about equal probability from addition to either carbon atom of the double bond. In our calculations it can be seen that $O(^3P)$ can be added to either carbon atom of the double bond of the propene and the addition to the methylene carbon is only slightly preferred.

After TS1 and TS2, two lower-energy adducts, IM1 and IM2, are formed, which have the relative energies of −24.41 and −24.72 kcal/mol, respectively. The similar stability of IM1 and IM2 also implies that the probability of the addition of $O(^3P)$ atom to either carton atom of the double bond is about equal.

In $CH_3CH{=}CH_2$ molecule, there are four different H atoms and all these H-abstraction reactions from $CH_3CH{=}CH_2$ by $O(^3P)$ are considered. First, the H-abstraction can occur from CH_2 group via TS3 as well as TS4, which directly correlate to products of $OH+CH_3CHCH$(I) and $OH+CH_3CHCH$(II) (as shown in Fig. 1). The two transition states have high relative energy of 20.08 and 19.41 kcal/mol, respectively, above the initial reactants. Second, CH_2CHCH_2 can be formed by H-abstraction from CH_3 group via TS5 with 16.02 kcal/mol higher in energy than that of the reactants. For the last H loss from CH group, 17.16 kcal/mol barrier is needed to overcome for this process to form CH_3CCH_2+OH via TS6. From Table 2, it can be seen that the imaginary frequencies of the transition states TS3, TS4, TS5 and TS6 are 1883.0i, 1900.5i, 1997.8i and 1970.3i cm^{-1} at the UMP2(full)/6-311G(d,p) level, respectively. The imaginary frequency plays an important role in the tunneling calculations, especially when it is large. It is found that the tunneling effect is significant at low temperatures for these reaction channels. Nevertheless, from the results calculated above it can be seen that the different H-abstraction channels from C_3H_6 by $O(^3P)$ face much higher barriers of about 16–20 kcal/mol, whereas the barriers of the addition steps are only ~0.5 kcal/mol. So the H-abstraction reactions cannot compete with the addition steps at low to fairly high temperatures and they are not discussed in the kinetic section.

Starting from IM1, there are five possible reaction pathways: (i) it can dissociate into the products CH_3CH+H_2CO via TS7 with a barrier height of 24.49 kcal/mol; (ii) with the cleavage of the C7–H8 bond, the products of $H+CH_3CHC(O)H$ will be formed via TS8, whose barrier is 22.48 kcal/mol; (iii) with the oxygen atom attached to C7 shifting from C7 to C5, IM1 will dissociate into CH_3 and epoxy ethane radical with the rupture of the C1–C5 bond and the corresponding transition state TS9 has a very high barrier of 62.75 kcal/mol, and so high a barrier indicates that this process from IM1 is negligible; (iv) IM1 can undergo a 1,2-H shift from C7 to C5, facing a high barrier of 34.76 kcal/mol via TS10 to form the biradical IM3

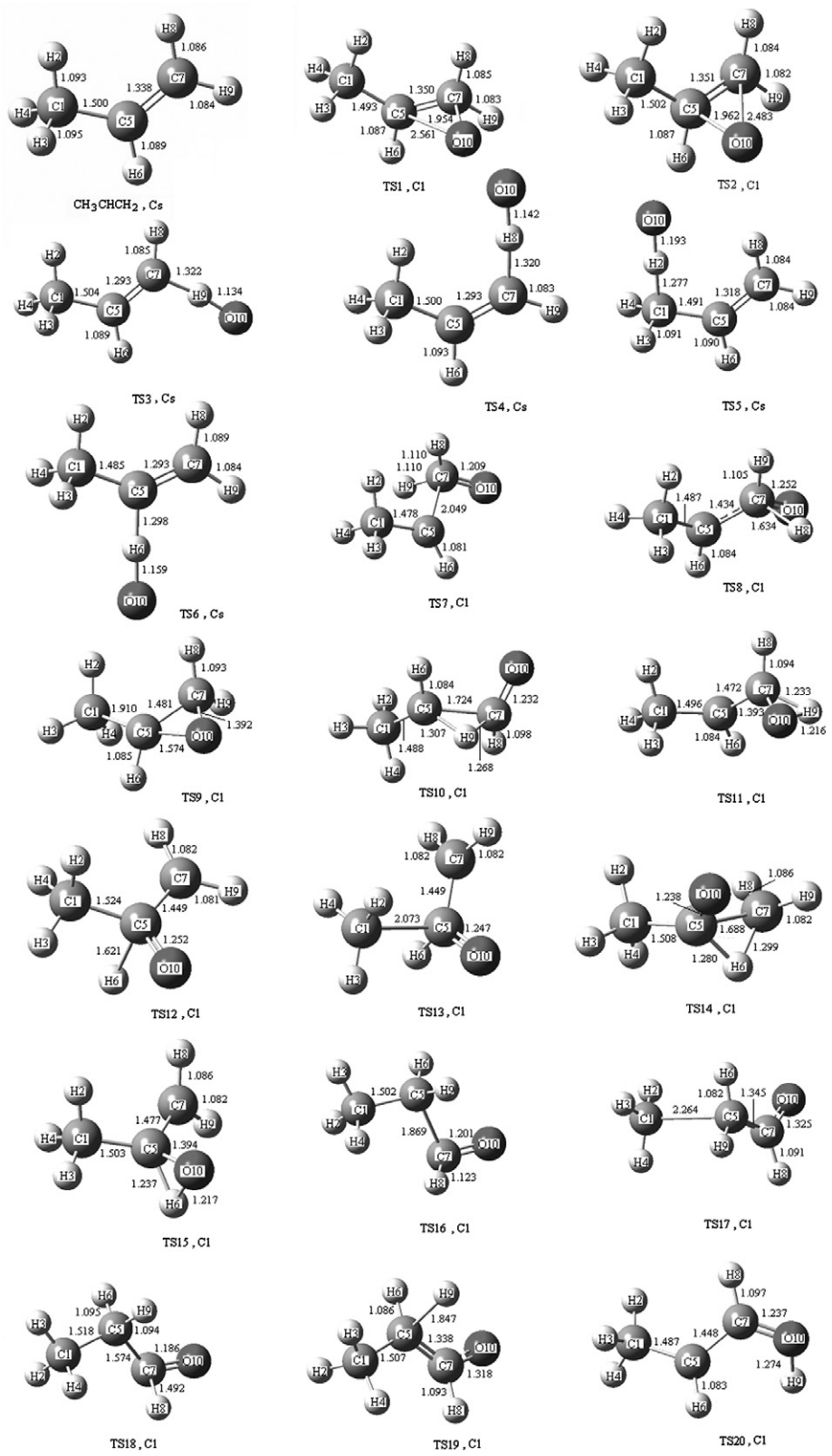

Fig. 1. Optimized geometries for reactants, the transition structures, intermediates, and products in the $O(^3P)+CH_3CHCH_2$ reaction. Bond lengths are given in angstrom.

(CH_3CH_2CHO); and finally, (v) IM1 can also isomerize to triplet IM4 by 1,2-H migration from C7 to O10 over a high barrier of 33.54 kcal/mol (TS11). It can be seen from Fig. 2 that the lower barrier dissociation reactions of producing CH_3CH+H_2CO and $H+CH_3CHC(O)H$ will far outrun the isomerizations. Moreover, the isomerization TSs lie

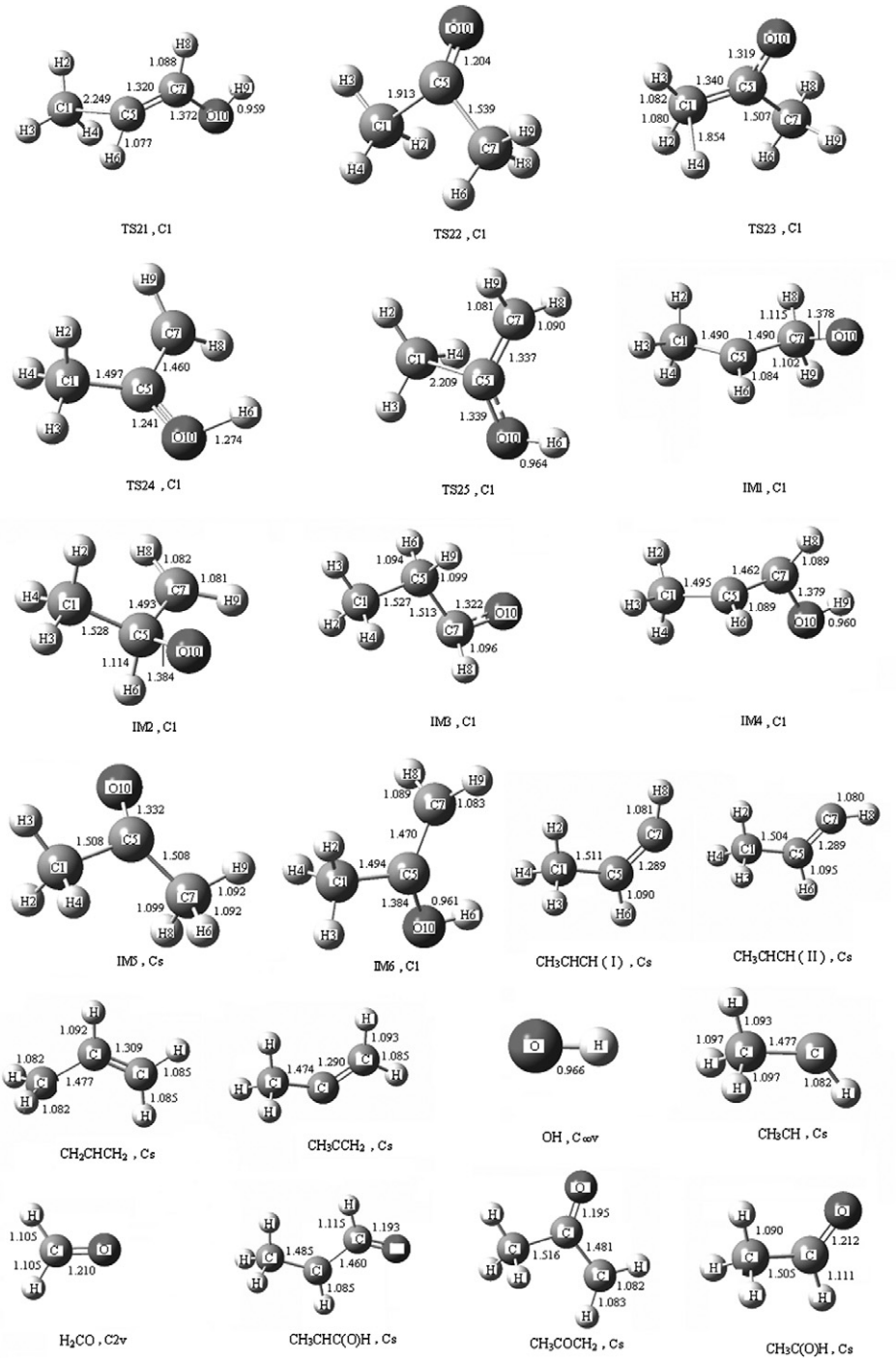

Fig. 1 (*continued*)

even above the entrance transition states, it is justifiable to neglect these steps in our kinetic analysis in the next section.

Similar to IM1, IM2 also has five different reaction pathways. IM2, with its energy 24.72 kcal/mol lower than that of the initial reactants, will rapidly dissociate into products of CH_3+$CH_2C(O)H$ via transition state TS13, whose barrier height is only 14.39 kcal/mol. The secondary feasible decomposition channel of IM2 is the formation of CH_3COCH_2+H with a lower barrier height of 22.51 kcal/mol via TS12. With the cleavage of the C5–C7 bond, the products of CH_2+$CH_3C(O)H$ will be formed from IM2 without any barrier. Besides the three dissociation pathways, two different hydrogen migrations can also occur from IM2. One is the 1,2-H shift from C5 to C7 to form IM5 via TS14 with a barrier height of 33.80 kcal/mol; and the other is the migrating H atom shifting from C5 to O10 via TS15 (which is 31.51 kcal/mol higher in energy

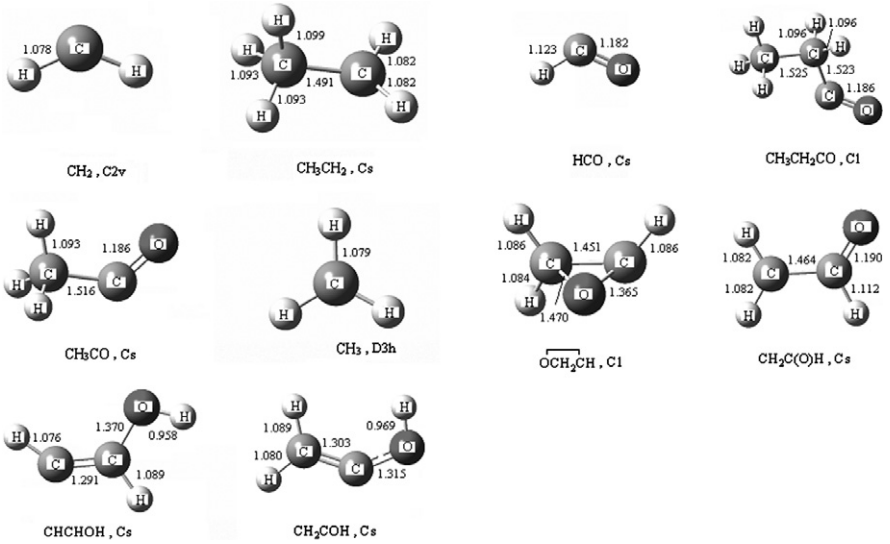

Fig. 1 (*continued*)

than that of IM2) to form IM6. IM5 and IM6 are the lowest-energy isomers of IM2 with relative energies of 37.12 and 37.48 kcal/mol lower than that of the reactants, respectively. As can be seen from Fig. 2, the dissociation products of CH_3+$CH_2C(O)H$ are found to be major and predominant on the triplet potential energy surface, while the formation of H dissociated from IM1 and IM2 will be the secondary product channels, and these conclusions are in good agreement with the experimental results [7–9,14].

From Fig. 2, it can be seen that in spite of the high isomerzation barriers, the isomers of IM3 and IM4 initiated from IM1, and IM5 and IM6 initiated from IM2 are ones with the lowest energy and once they have been formed, a series of subsequent reactions will occur as discussed below.

Triplet IM3 can decompose via four different channels, of which the channel via TS16 leading to CH_3CH_2+HCO is predominant because of its lower barrier height of 13.53 kcal/mol. We should note that the energy of TS16 is lower than that of the products of CH_3CH_2+HCO at the QCISD(T)/6-311++G(3df,2p) level. This may be caused by the fact that the energy calculated at the QCISD(T)/6-311++G(3df,2p) level for a UMP2-optimized geometry does not correspond exactly to the top of the saddle point. For the rupture of the C1–C5 single bond, 42.20 kcal/mol barrier is needed to overcome via TS17 to form CH_3+$CH_2C(O)H$. Two H-loss reaction pathways from IM3 are also found. One is the cleavage of the C–H bond in the CHO group to form CH_3CH_2CO+H via TS18 with a lower barrier height of 25.80 kcal/mol; and the other is the departure of the H atom from CH_2 group to form CH_3CHCHO+H via TS19 with a higher barrier height of 43.64 kcal/mol.

Only two dissociation pathways from IM4 have been found. One is the formation of $CH_3CHC(O)H$+H via transition state TS20. Although TS20 has a barrier height of 38.17 kcal/mol, as shown in Table 1 and Fig. 2, it is only 3.19 kcal/mol above the energy of the reactants at the QCISD(T)/6-311++G(3df,2p) level and this pathway is effectively available in the title reaction. The other dissociation pathway of IM4 is to produce CH_3+CHCHOH via TS21, which has a higher barrier of 52.44 kcal/mol, and it is well above the energy available in the reaction at normal temperatures and thus it is not discussed further.

If triplet IM5 is formed, the dissociation channel that produces CH_3+CH_3CO via TS22 will be the predominant one because of its lower barrier height of 16.91 kcal/mol, whereas the formation of CH_3+CHCHOH, which faces a high barrier of 54.25 kcal/mol via TS23, is negligible.

Starting at triplet IM6, there are two dissociation channels to form CH_3COCH_2+H and CH_3+CH_2COH via TS24 and TS25, whose barrier heights are 39.44 and 51.74 kcal/mol, respectively. The energy of TS24 is only 1.96 kcal/mol higher than that of the reactants. This indicates the feasibility of this channel. As a contrast, the higher barrier of TS25 prevents the further reaction process.

As shown in Fig. 2, the formations of IM1 and IM2 initiated from reactants are feasible because of their lower barrier heights, and the dissociation channels of producing CH_3+$CH_2C(O)H$ from IM2 will be the dominant one and the formations of CH_3COCH_2+H from IM2 together with $CH_3CHC(O)H$+H from IM1 will be the secondary ones.

3.2. Rate constants

Based on the information obtained from the potential energy surface, the addition of O(^{3}P) atom to the double bond are the rate controlling steps in the overall reaction. The rate constants for the initial addition channels are calculated. The rate constants are evaluated by means of conventional transition state theory (TST) [18–20] expression:

Table 1
Calculated relative energy (kcal/mol) for various fragments in the $O(^3P)+CH_3CHCH_2$ reaction using different levels of theory

Species	ΔE, ZPE	ΔE, UMP2(full)/BS1[a]	ΔE, UMP2(full)/BS2[b]	ΔE, QCISD(T)/BS1[a]	ΔE, QCISD(T)/BS2[b]
CH3CHCH2+O(3P)	0.00	0.00	0.00	0.00	0.00
IM1	0.71	−17.31	−23.64	−18.08	−24.41
IM2	0.42	−18.33	−24.28	−18.77	−24.72
IM3	1.87	−23.03	−29.99	−25.83	−32.79
IM4	1.19	−28.62	−38.15	−25.45	−34.98
IM5	1.71	−27.28	−34.63	−29.77	−37.12
IM6	0.91	−31.83	−41.10	−28.22	−37.48
TS1	0.81	13.52	8.60	5.43	0.51
TS2	0.89	13.87	8.92	5.52	0.57
TS3	−2.81	23.21	21.70	21.59	20.08
TS4	−2.69	22.46	21.25	20.61	19.41
TS5	−1.29	17.95	15.75	18.22	16.02
TS6	−2.71	20.51	18.64	19.02	17.16
TS7	−1.12	7.91	1.98	6.01	0.08
TS8	−3.53	0.13	−3.57	1.77	−1.93
TS9	−0.64	46.73	37.52	47.55	38.34
TS10	−1.80	15.09	8.19	17.26	10.35
TS11	−1.83	12.03	5.42	15.74	9.13
TS12	−3.54	−0.34	−4.06	1.52	−2.21
TS13	−1.43	−1.85	−7.55	−4.64	−10.33
TS14	−1.83	13.90	6.77	16.21	9.08
TS15	−2.14	9.12	2.60	13.32	6.79
TS16	−0.01	−12.02	−19.12	−12.16	−19.26
TS17	−1.46	20.13	15.56	13.97	9.41
TS18	−2.58	−6.11	−10.46	−2.65	−6.99
TS19	−3.23	21.44	13.69	18.59	10.85
TS20	−2.64	8.95	−0.03	12.17	3.19
TS21	−1.89	25.44	18.41	24.50	17.46
TS22	−0.06	−11.84	−19.39	−12.66	−20.21
TS23	−3.44	15.37	13.93	18.56	17.13
TS24	−3.46	5.22	−2.71	9.90	1.96
TS25	−1.76	21.52	15.02	20.76	14.26
$CH_3CHCH(I)+OH$	−2.14	20.27	17.21	18.57	15.51
$CH_3CHCH(II)+OH$	−2.25	19.69	16.74	18.20	15.25
$CH_2CHCH_2(Cs)+OH$	−1.38	9.91	5.57	10.95	6.61
CH_3CCH_2+OH	−2.34	16.03	12.75	14.99	11.71
CH_3CH+H_2CO	−3.09	−6.55	−8.21	0.37	−1.29
$CH_3CHC(O)H+H$	−4.96	−13.93	−16.46	−6.07	−8.60
$CH_3C(O)H+CH_2$	−4.02	−12.67	−13.32	−3.77	−4.41
CH_3COCH_2+H	−5.28	−17.15	−19.46	−7.40	−9.71
CH_3CH_2+HCO	−4.13	−25.94	−26.58	−17.91	−18.55
CH_3CH_2CO+H	−4.58	−24.90	−25.92	−11.62	−12.63
CH_3+CH_3CO	−4.03	−32.09	−33.80	−24.00	−25.72
$CH_3+\overline{OCH_2CH}$	−3.33	13.56	8.23	20.59	15.25
$CH_3+CH_2C(O)H$	−4.22	−16.43	−19.20	−14.15	−16.92
$CH_3+CHCHOH$	−3.64	15.67	10.65	18.21	13.18
CH_3+CH_2COH	−4.31	8.05	4.73	13.05	9.73

[a] BS1 means 6-311G(d,p) basis set.
[b] BS2 means 6-311++G(3df,2p) basis set.

$$k = k^{W} \cdot \sigma \cdot \frac{k_B T}{h} \cdot \frac{Q_{TS}}{Q_{Rct}} \cdot \exp\left(-\frac{\Delta E^{\neq}}{RT}\right)$$

in which Q_{TS} and Q_{Rct} are the partition functions of the transition state and reactants, k^W is a tunneling factor, σ is the symmetry factor accounting for the possibility of more than one symmetry-related reaction path, k_B is Boltzmann's constant, h is Planck's constant, and $\Delta E^{\neq}$ are the barrier heights of 0.51 and 0.57 kcal/mol of TS1 and TS2 for the initial addition channels, respectively. The total partition function is given by the product of translational (Q_{trans}), rotational (Q_{rot}), vibrational (Q_{vib}) and electronic (Q_{elec}) partition function. The partition functions are evaluated using UMP2(full)/6-311G(d,p) moments of inertia and UMP2(full)/6-311G(d,p) frequencies (scaled by 0.95) using standard formulas. Table 2 shows frequencies and

Table 2
Scaled harmonic frequencies[a] and rotational constants[b] calculated at the UMP2(full)/6-311G(d,p) level of theory

Species	Frequencies	Rotational constants		
		I_x	I_y	I_z
CH_3CHCH_2	189.9, 403.2, 553.6, 863.5, 896.4, 903.6, 975.7, 1022.2, 1140.0, 1258.1, 1349.1, 1390.0, 1422.7, 1438.5, 1623.6, 2920.6, 2992.7, 3011.9, 3022.5, 3034.5, 3117.9	46.29462	9.31827	8.14838
TS1	656.8i[c], 123.1, 148.4, 241.9, 410.4, 648.4, 890.3, 902.1, 970.9, 988.2, 1019.8, 1152.7, 1252.4, 1347.1, 1387.9, 1420.2, 1436.1, 1559.5, 2922.5, 2994.4, 3022.9, 3041.3, 3061.7, 3128.6	14.23096	4.68828	4.02443
TS2	653.9i[c], 173.1, 221.0, 259.2, 403.3, 570.9, 867.8, 895.4, 910.6, 993.4, 1031.3, 1150.7, 1242.8, 1345.9, 1396.4, 1425.5, 1440.4, 1541.4, 2936.3, 3017.3, 3037.7, 3047.6, 3059.1, 3151.8	8.75199	7.52424	4.66986
TS3	1883.0i[c]			
TS4	1900.5i[c]			
TS5	1997.8i[c]			
TS6	1970.3i[c]			
TS7	557.6i [c]			
TS8	1226.4i[c]			
TS9	1108.2i[c]			
TS10	1430.3i[c]			
TS11	2082.0i[c]			
TS12	1276.0i[c]			
TS13	589.5i[c]			
TS14	1406.1i[c]			
TS15	2044.7i[c]			
TS16	504.0i[c]			
TS17	628.6i[c]			
TS18	1558.6i[c]			
TS19	1094.3i[c]			
TS20	4933.8i[c]			
TS21	933.3i[c]			
TS22	686.9i[c]			
TS23	1059.2i[c]			
TS24	4266.8i[c]			
TS25	1017.1i[c]			

[a] Unit in cm^{-1}. Scaled by a factor of 0.95 to account for the anharmonic effects.
[b] Unit in GHz.
[c] Imaginary frequency.

moments of inertia of reactants, TS1, and TS2 calculated at UMP2(full)/6-311G(d,p) level of theory. The O(^{3}P) atom has a large electronic partition function due to the spin-orbital splitting of the ^{3}P level. The electronic partition function of the O(^{3}P) atom explicitly includes the three lowest-lying electronic states ($^3P_2$, $^3P_1$ and $^3P_0$), $Q_e = 5.0 + 3.0 \times \exp(-158.5\ cm^{-1}/(RT)) + \exp(-226.5\ cm^{-1}/(RT))$ [10,21]. In addition, the electronic degeneracy of 3 for TS1 and TS2 is also taken into account. The level of tunneling calculation is the corresponding Wigner's tunneling correction [22,23]:

$$k^W = 1 + \frac{1}{24}\left(\frac{h\upsilon^{\neq}}{k_B T}\right)^2$$

where k^W is the Wigner correction factor, and $\upsilon^{\neq}$ is the imaginary frequency at the saddle point.

It can be seen from Table 2, the imaginary frequency of the transition state TS1 is 656.8i cm^{-1} at the UMP2(full)/6-311G(d,p) level. The Wigner correction factor increases the rate constant for TS1 by factors of 1.42 at $T = 298$ K, 1.23 at $T = 400$ K, and 1.15 at $T = 500$ K. As we can see, the Wigner correction factor decreases as the temperature increases. It is found that the tunneling effect is not significant at low temperatures for this reaction channel. The imaginary frequency of the transition state TS2 is 653.9i cm^{-1} at the UMP2(full)/6-311G(d,p) level. The value of 653.9i cm^{-1} leads to the conclusion that tunneling is of little importance in the low temperature range.

We have computed overall thermal rate constants in the wide range of temperature 298–500 K. These are listed in Table 3, together with some of the experimental data available for comparison. It is obvious that the calculated data are in quite good agreement with the experimental values over the temperature range. At room temperature, our computed rate constant of 1.80×10^{-12} cm^3 $molecule^{-1}$ s^{-1} is in agreement with a recently recommended value of 3.93×10^{-12} cm^3 $molecule^{-1}$ s^{-1} [24]. Using our computed data at temperatures between 298 and 500 K, we fit our $k_{overall}$ to an Arrhenius expression as: $k(T) = 5.43 \times 10^{-12}$ (cm^3 $molecule^{-1}$ s^{-1}) $\times$ $\exp(-0.67\ kcal\ mol^{-1}/RT)$, which agrees well with the experimentally derived a rate expression of $k = (10.1 \pm 1.5) \times 10^{-12}$ (cm^3 $molecule^{-1}$ s^{-1}) exp $(-(0.56 \pm 0.20)$ kcal $mol^{-1}/RT)$ [24]. Moreover, the calculated activation energy, 0.67 kcal mol^{-1}, produced by the calculation in the temperature range 298–500 K agrees with the experimental value of (0.56 ± 0.20) kcal mol^{-1}, too.

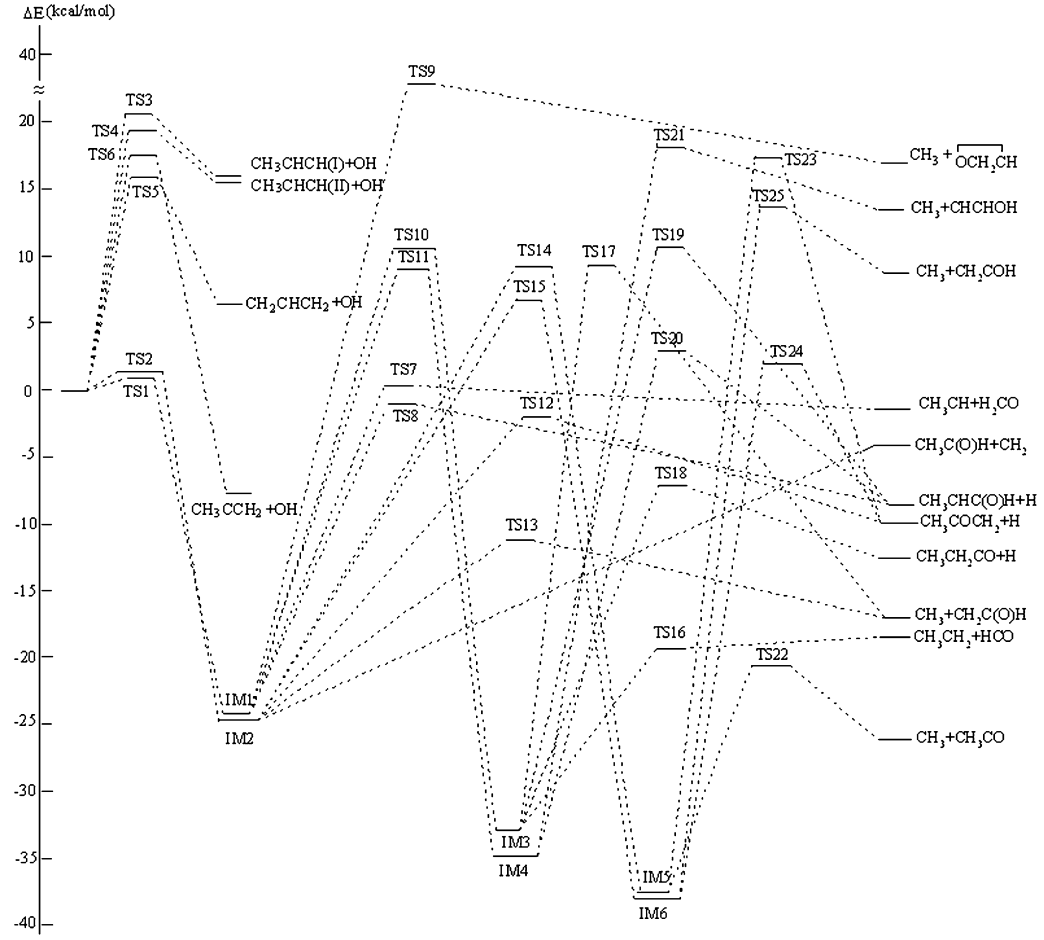

Fig. 2. Energetic profile (kcal/mol) for the triplet potential energy surface of the $O(^3P)+CH_3CHCH_2$ reaction at the QCISD(T)/6-311++G(3df,2p) level.

Table 3
Calculated rate constants ($cm^3\,molecule^{-1}\,s^{-1}$) for the $O(^3P)+CH_3CHCH_2$ reaction over the temperature range 298–500 K

T/K	k_{TS1}	k_{TS2}	$k_{overall}$	$k_{exp.}$ [24]
298	1.19E-12	6.15E-13	1.80E-12	3.93E-12
310	1.23E-12	6.32E-13	1.86E-12	4.07E-12
320	1.26E-12	6.47E-13	1.90E-12	4.19E-12
330	1.29E-12	6.62E-13	1.95E-12	4.30E-12
340	1.32E-12	6.77E-13	2.00E-12	4.41E-12
350	1.35E-12	6.93E-13	2.05E-12	4.52E-12
360	1.39E-12	7.09E-13	2.10E-12	4.62E-12
370	1.42E-12	7.25E-13	2.15E-12	4.72E-12
380	1.45E-12	7.42E-13	2.20E-12	4.82E-12
390	1.49E-12	7.59E-13	2.25E-12	4.91E-12
400	1.52E-12	7.76E-13	2.30E-12	5.00E-12
420	1.59E-12	8.11E-13	2.40E-12	5.17E-12
440	1.67E-12	8.47E-13	2.51E-12	5.33E-12
460	1.74E-12	8.83E-13	2.62E-12	5.48E-12
480	1.82E-12	9.21E-13	2.74E-12	5.62E-12
500	1.89E-12	9.60E-13	2.85E-12	5.75E-12

4. Conclusion

In the present work, the mechanisms of the complex multichannel reaction of $O(^3P)+CH_3CH{=}CH_2$ are revealed theoretically for the first time. The potential energy profile of various possible reaction channels is evaluated at the QCISD(T)/6-311++G(3df,2p) level. Our calculations indicate that the initial addition of $O(^3P)$ to either carbon atom of the double bond is about equal and the major product channel is the formation of $CH_3+CH_2C(O)H$ from IM2, whereas CH_3COCH_2+H from IM2 and $CH_3CHC(O)H+H$ from IM1 are minor channels. The detailed kinetics calculations for the two processes are carried out. Conventional transition state theory has been used for the calculation of the rate constant for the initial addition channels in the temperature range 298–500 K, including Wigner's tunneling correction. The calculated rate constants agree very well with experimental values available.

References

[1] D. Saunders, J. Heicklen, J. Phys. Chem. 70 (1966) 1950.
[2] R.J. Cvetanovic, J. Phys. Chem. 74 (1970) 2730.
[3] M.D. Scheer, R. Klein, J. Phys. Chem. 74 (1970) 2732.
[4] R.E. Huie, J.T. Herron, Prog. React. Kinet. 8 (1978) 1.
[5] M.C. Lin, in: K.P. Lawley (Ed.), Potential Energy Surfaces, Wiley, New York, 1980, p. 136.
[6] R.J. Cvetanovic, Prog. React. Kinet. 2 (1964) 39.
[7] K. Kleinermanns, A.C. Luntz, J. Phys. Chem. 85 (1981) 1966.

[8] R. Quandt, Z.Y. Min, X.B. Wang, R. Bersohn, J. Phys. Chem. A. 102 (1998) 60.
[9] H.M. Su, R. Bersohn, J. Phys. Chem. A. 105 (2001) 9178.
[10] T.L. Nguyen, L. Vereecken, X.J. Hou, M.T. Nguyen, J. Peeters, J. Phys. Chem. A 109 (2005) 7489.
[11] H.M. Zhao, W.S. Bian, K. Liu, J. Phys. Chem. A 110 (2006) 7858.
[12] V.D. Knyazev, V.S. Arutyunov, V.I. Dedeneev, Int. J. Chem. Kinet. 24 (1992) 545.
[13] R.B. Klemm, R.P. Thorn Jr., S.C. Kuo, S.K. Ross, Chem. Phys. Process. Combust. (2001) 122–123.
[14] V.S. Arutyunov, V.I. Vedeneev, V.D. Knyazev, Khim. Fiz. 9 (1990) 1383.
[15] C. Möller, M.S. Plesset, Phys. Rev. 46 (1934) 618.
[16] C. Gonzalez, H.B. Schlegel, J. Chem. Phys. 90 (1989) 2154.
[17] M.J. Frisch et al., Gaussian 03 Revision B. 05, Gaussian Inc., Pittsburgh, PA, 2003.
[18] A.D. Isaacson, D.G. Truhlar, J. Chem. Phys. 90 (1989) 1007.
[19] T. Yamada, T.D. Fang, P.H. Taylor, R.J. Berry, J. Phys. Chem. A 104 (2000) 5013.
[20] T.D. Tzima, D.K. Papayannis, V.S. Melissas, Chem. Phys. 312 (2005) 169.
[21] B.S. Wang, H. Hou, Y.S. Gu, J. Phys. Chem. A 103 (1999) 2060.
[22] S.M. Resende, F.R. Ornellas, Chem. Phys. Lett. 318 (2000) 340.
[23] E.P. Wigner, Z. Phys. Chem. Abt. B 19 (1932) 203.
[24] R.J. Cvetanovic, J. Phys. Chem. Ref. Data 16 (1987) 261.